Available online at www.sciencedirect.com

jmr&t Journal of Materials Research and Technology

journal homepage: www.elsevier.com/locate/jmrt

Original Article

Microstructural characterisation and hardness assessment of wire arc cladded Hastelloy C276 on creep resistant steel P91

Bintao Wu [a,b], *Zhijun Qiu* [b,*], *Bosheng Dong* [b], *Ondrej Muránsky* [c], *Hanliang Zhu* [b,c], *Zhiyang Wang* [c], *Zengxi Pan* [b], *Huijun Li* [b]

[a] *School of Materials and New Energy, Ningxia University, Yinchuan 750400, China*
[b] *School of Mechanical, Materials, Mechatronic and Biomedical Engineering, University of Wollongong (UOW), Wollongong, NSW 2522, Australia*
[c] *Australian Nuclear Science and Technology Organisation (ANSTO), Sydney, NSW 2234, Australia*

ARTICLE INFO

Article history:
Received 18 April 2022
Accepted 23 June 2022
Available online 30 June 2022

Keywords:
Steel-nickel metal cladding
Interface
Grain features
Microhardness

ABSTRACT

A new structure with nickel-based Hastelloy C276 alloy cladding on creep resistant steel P91 was developed in this study for nuclear applications. The microstructure, including precipitation and grain size, boundaries, orientation and hardness distribution of cladding structures with/without post heat treatment were explored using a range of microscopy techniques and hardness testing. The results show that the as-cladded structure exhibits highly hierarchical heterogeneity, which is mainly related to the remarkably coarse-grained microstructure in the heat-affected zone on the steel side, and typically columnar dendrites formed on the Hastelloy side. After tempering heat treatment, the specimen exhibits re-orientated grains and homogenized microstructure. Meanwhile, the ratio of high angle grain boundaries (HAGBs) in steel regions significantly increases, and the hardness values turn even distribution. This study achieves a sound metallurgical bonding between two structural materials and offers insights into the development of dissimilar metal components with in-site specific properties.
© 2022 The Author(s). Published by Elsevier B.V. This is an open access article under the CC BY-NC-ND license (http://creativecommons.org/licenses/by-nc-nd/4.0/).

1. Introduction

Dissimilar metals have been widely applied in industrial sectors, such as the defence, energy, transportation and aerospace [1,2]. At present, one of the main impediments to the dissimilar metal design is the atomic dilution of metals in interfacial regions, leading to the potential formation of detrimental brittle intermetallic compounds (IMCs) [3]. Extensive studies have been undertaken to develop manufacturing processes or approaches that are capable of producing advanced bimetallic materials with desired functionalities. Additive manufacturing (AM) techniques, where materials are introduced to parts sequentially, provide

* Corresponding author.
E-mail address: zq145@uowmail.edu.au (Z. Qiu).
https://doi.org/10.1016/j.jmrt.2022.06.129
2238-7854/© 2022 The Author(s). Published by Elsevier B.V. This is an open access article under the CC BY-NC-ND license (http://creativecommons.org/licenses/by-nc-nd/4.0/).

exciting opportunities for producing high-quality dissimilar metal components with discrete properties in an integrated manner. This can be achieved by tailoring local chemical composition distribution in components to eliminate detrimental IMCs formation via manipulating local feedstocks during AM.

Ni-based superalloys are desirable materials for structural applications in future Generation IV nuclear reactors, such as supercritical water-cooled reactor (SWCR) and molten salt reactor (MSR), due to their superior corrosion resistance and excellent mechanical properties at ambient and elevated temperatures. Hastelloy C276 alloy is a solid solution strengthened Ni-based superalloy and it has superior high-temperature stability, high-temperature oxidation resistance and corrosion resistance [4,5]. These properties enable this alloy for a wide range of applications in nuclear and chemical industries under high temperature or harsh environmental conditions, such as SWCR and flue gas desulfurization systems [6]. This alloy consists of high content of Mo and Cr alloying elements that are usually coherent with topologically closed packed (TCP) intermetallic precipitates of *p* phases under as-fabricated conditions [7]. In general, Hastelloy C276 is observed to be readily weldable, however, due to the rapid precipitation of hard and brittle intermetallics during the welding process, the weldment is possible to have cracking or deteriorated properties. Hence, there requires a critical control for the welding of Hastelloy C276 components to impede *p* phase precipitation.

P91 steel is a type of 9Cr–1Mo steel with deliberate addition of V and Nb elements, and it has an outstanding heat resistance and creep strength while suffering from relatively low corrosion resistance. This alloy is primarily used for the superheater and reheater in power plant boiler construction, and heating furnace piping in the petrochemical industry, with a steam temperature of around 650 °C and pressure of 30 MPa [8]. P91 steel has a typical tempered martensitic structure, which may be further decomposed during long-term service at elevated temperatures. Meanwhile, it often faces the challenge of property degradation [9]. To maintain required mechanical properties at high temperatures, several attempts have been directed towards modifying P91 steel through the addition of N or carbonitride elements, which promote the precipitation of carbonitride particles or fine carbides in material [10]. However, the use of P91 steel is limited at a temperature above 650 °C due to its limitation in oxidation resistance.

Although Hastelloy C276 alloy and P91 steel are both suitable for a high-temperature application, Hastelloy alloy exhibits much better corrosion and oxidation resistance but suffers from higher production costs compared to P91 steel. Cladding Hastelloy C276 on P91 steels has great potential to produce a component with both excellent high-temperature mechanical properties and oxidation/corrosion resistance in a cost-effective manner, which presents attractive nuclear application significance under elevated temperatures. The operational strategy involves a new hierarchically-heterogenous Ni-based alloy-steel structure that offers specific properties to severe environments. Since both Hastelloy C276 alloy and P91 steel exhibit good weldability, these two materials are potential candidate materials that can be further joined using wire arc additive manufacturing (WAAM) method to create a structural part. Here the WAAM technique offers flexibility for producing cladding materials at specific locations of a component and modifying the interfacial microstructure to achieve good bonding. Sridar et al. [11] reported a P91 steel - Inconel 740H bimetallic structure fabricated using WAAM, while they found the crack is susceptible to being generated in gradient regions. The cracking susceptibility represents a major challenge for achieving reliable applications of these promoted P91 steel and nickel-based alloy parts during fabrication.

To explore the fabrication of more reliable structural materials, this study focuses on the development of a new dissimilar metal structure where Hastelloy C276 is cladded on P91 steel for nuclear application. Here a sound metallurgical bonding between two structural materials was achieved, and the material characterization was explored under both as-cladded and heat-treated conditions. The challenges potentially occurring in dissimilar structures, especially cracking and unhomogenized microstructures, have been addressed. This work provides insights into the development of dissimilar metal cladding with in-site specific properties.

2. Materials and methods

The P91 steel was in normalized and tempered condition, and it was cut to a substrate plate with dimension of 100 mm × 50 mm × 6 mm. The Hastelloy C276 welding wire, with a diameter of 1.2 mm, were used as the feedstocks and it was cladded on steel substrate using a Gas Tungsten Arc Welding (GTAW) based WAAM system, as shown in Fig. 1. The chemical compositions of studied materials are listed in Table 1. The process parameters used for cladding were kept constant, with a welding arc current of 140 A, an arc voltage of 13.0 V, a torch travel speed of 100 mm/min, a wire feed speed of 1000 mm/min, and a tungsten tip to workpiece distance of 3 mm. High purity argon (99.99%) was utilized at a flow rate of 15 L/min for welding torch and trailing shielding gas cover. The interval time between each cladding layer was maintained at approximately 30 s. After the cladded part was produced, specimens were extracted from the cladded plate mid-section for tempering treatment, which was carried out at 760 °C for 2 h in a vacuum furnace, followed by air cooling.

The metallographic specimens were hot mounted, ground and polished according to the standard procedures. After that, the specimens were etched in the Villela's reagent (95 ml ethanol, 5 ml hydrochloric acid and 1 g picric acid) for steel microstructure observation, and then electro-etched in a mixed solution (5 mg oxalic acid and 15 ml hydrochloric acid) with 6 V direct current for 2 s at room temperature to reveal hastelloy microstructure features. The microstructure were examined using a Leica M205A deep field stereoscopic microscope and a JEOL JSM-7001 scanning electron microscope (SEM) equipped with an energy dispersive X-ray spectroscopy (EDS) detector. Electron Back-Scattered Diffraction (EBSD) analyses were performed using a Zeiss® Ultra Plus SEM. The collected EBSD data were analyzed using the MTEX package [12]. Vickers hardness was measured on the same metallographic specimens, using a Matsuzawa Via-F automatic Vickers hardness tester, at a test load of 1 kg, an indentation

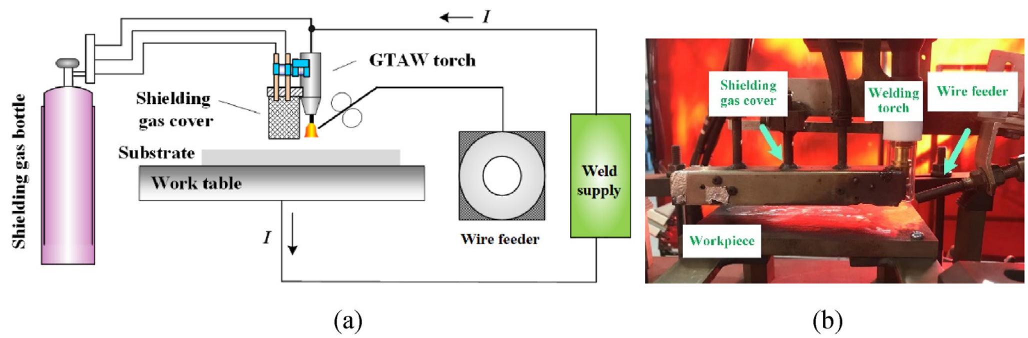

Fig. 1 – WAAM system used in this study: (a) schematic diagram; (b) experiment setup.

dwelling time of 15s, and a step size of 0.5 mm, in accordance with the ASTM E384 standard. A hardness map was further drawn to depict hardness distributions from cladded Hastellloy layer to steel substrate.

3. Results and discussion

3.1. *Metallographic observations*

Fig. 2 shows cross-sectional macrographs and high-magnification micrographs at the representative locations in as-cladded and heat-treated conditions. As can be seen, no macro-scale defects, including pores, cracks, or insufficient fusion, were observable on macrographs, which is favorable for practical application.

The coating layers (Hastelloy C276) exhibit a typical weld-like microstructure, comprising columnar dendrites with epitaxial or cellular morphologies, as shown in Fig. 2b. These columnar grains are recognized as the γ-Ni matrix, and it has been reported that dendrite generation in Hastelloy γ-Ni matrix often associated with solute element segregation during rapid solidification conditions [13]. Hence, the intermetallic *p* phase can be found in the interdendritic area, as shown in Fig. 3.

The heat-affected zone (HAZ) exhibits two distinct regions in as-cladded and heat-treated conditions: (i) coarse-grained HAZ (CGHAZ, Fig. 2c/h), and fine-grained HAZ (FGHAZ, Fig. 2d/i). The CGHAZ (Tp>>A_{c3}) and FGHAZ (Tp>A_{c3}) regions are formed due to the thermal cycling experienced during WAAM [14]. Here, Tp is the peak temperature experienced during deposition, and the temperature of A_{c3} for P91 steel is in the range of 890–940 °C [15]. The CGHAZ (Fig. 2c) regions are mainly composed of a typical lath martensitic microstructure with negligible precipitates. This region is close to the interface and experiences a temperature well above A_{c3} transformation temperature. As the Tp is much higher than the A_{c3} temperature in the CGHAZ region, the dissolution of the precipitates located along the prior martensite grain boundaries was promoted, leading to the grain boundary migration and resultant coarsening of prior grains during deposition [16]. It is evident that the CGHAZ often features the highest hardness of the HAZ [17], and this will be further presented in the following section. Moreover, the remelting from the subsequent thermal cycle also contributes to grains growth at the CGHAZ due to re-heating in this region. In contrast, The FGHAZ (Fig. 2d) experienced a peak temperature slightly higher or equal to the A_{c3} temperature, which leads to a complete phase transformation of austenite without significant grain growth, following the formation of fresh martensite during cooling, and then causing fine martensitic structure [17]. The substrate (P91 steel) shows highly tempered lath martensite together with a large amount of carbide precipitates located at both martensitic lath boundaries and prior austenite grain boundaries (Fig. 2e).

After heat treatment, grains appeared to be coarsened in the all regions (Figs. 2g–j), including the cladding layer, CGHAZ, FGHAZ, and substrate, compared with that of as-cladded condition. On the Hastelloy side, more *p* phase precipitates in the interdendritic area, as shown in Fig. 3. The *p* phase can strengthen the alloy at ambient temperature, but it has some adverse effects on corrosion resistance and hot cracking susceptibility [15]. On the steel side, tempering may result in the formation of new carbides and carbonitride precipitates at CGHAZ, and the main precipitates are widely reported to be Cr-enriched $M_{23}C_6$ and (Nb, V) enriched MX [14]. P91 steel has a narrow solidification temperature window to allow the material to solidify to the point that carbides become thermodynamically stable. Hence, these precipitates have a non-uniform distribution, and altered amounts or volume fractions, as shown in Fig. 2.

Fig. 4 shows a close observation of interfacial bounding regions for two specimens. As can be seen, Hastelloy coating presents obvious elemental segregation, especially Mo and W that congests along interdendritic boundaries. From EDS mapping, there is no discernible diffusion of main

Table 1 – Chemical compositions of materials (wt.%).

Composition	Ni	Mo	Cr	Fe	W	C	Mn	Co	V	P	Si
Wire (Hastelloy)	Bal.	16.5	16.0	5.8	4.0	0.01	0.19	0.20	0.06	0.015	0.08
Substrate(P91 steel)	0.17	0.9	8.65	Bal.	–	0.1	0.9	–	0.21	0.009	0.28

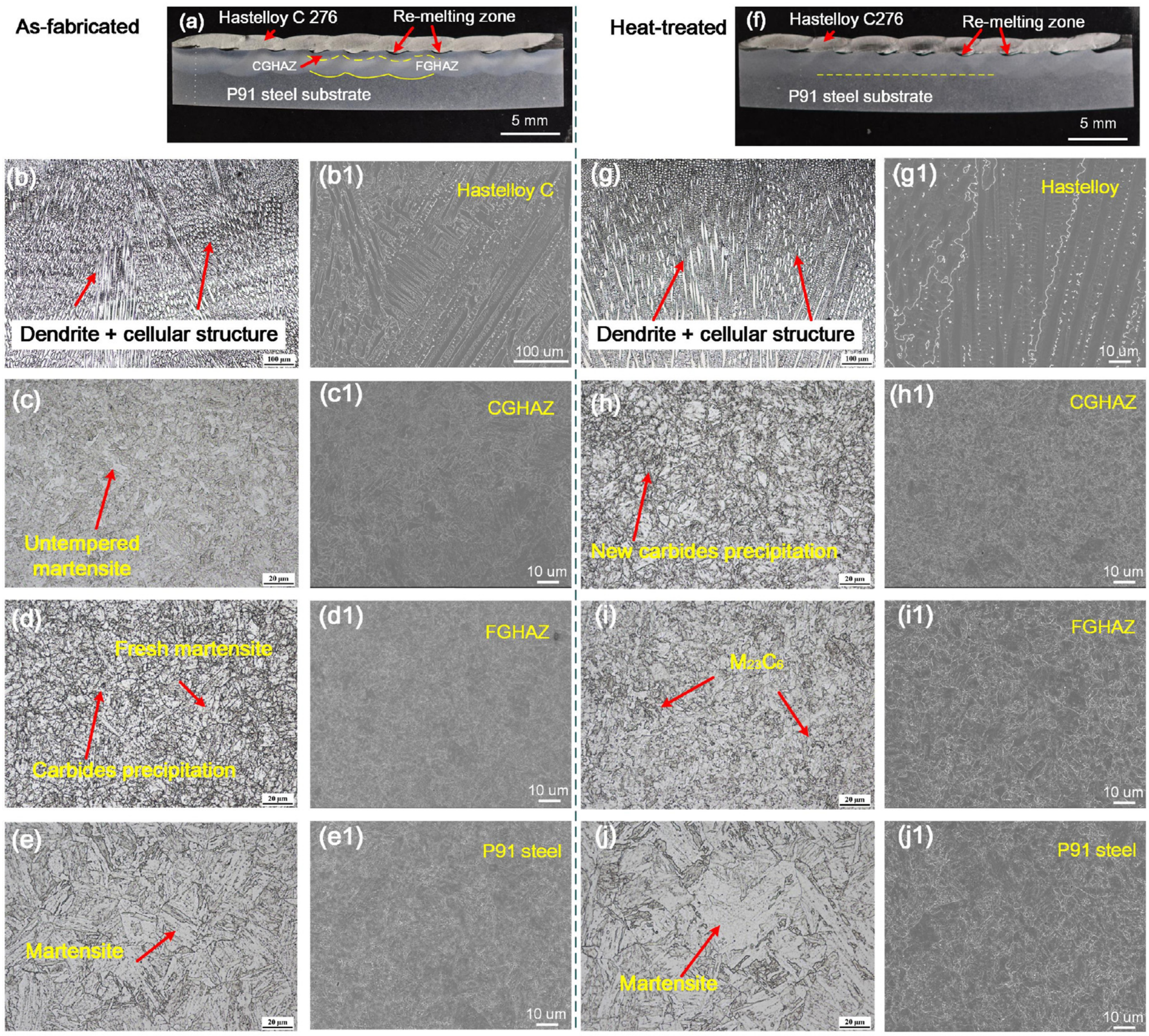

Fig. 2 – The cross-sectional macrographs of the specimens: (a) as-cladded; (f) heat-treated, and optical micrographs and SEM images of selected locations for the studied specimens: (b), (c), (d) and (e) as-cladded condition for Hastelloy C, CGHZZ, FGHAZ, substrate; (g), (h), (i) and (j) heat-treated condition for the corresponding regions as mentioned above.

constitution elements (Ni, Fe, Cr, Mo, W) between two materials, but inhomogeneous pervasion of minor alloying elements W, Si, Mn and Co appeared during the deposition process. The dispersion of W element contributed more carbide precipitations to substrate, which could further impede grain growth in heat-affected zones [18]. Meanwhile, this behaviour benefits improving the oxidation and carburization resistance of the cladding via the stabilization of primary carbides which are the strengthening phases in Ni-based alloys [19]. It is noticed that the Mn element has a significant dispersion into the Hastelloy side, especially after heat treatment. This behaviour is likely to improve the mechanical properties and oxidation resistance of the material [20].

On P91 steel side, as shown in Fig. 4, some δ-ferrite formed in CGHAZs in the vicinity of fusion line, which may be attributed to the carbon partitioning to Hastelloy C276 at high temperature and relatively high cooling rate after cladding [17]. It is observed that the mixing zones or remelting zones were generated near the interface (Fig. 4c). These mixing zones were promoted by the formation of a stagnant molten layer of the cladded material. As the overlapped path was used during WAAM, there will generate a mixing between the new layer and the adjacent deposited layer. It is well recognised that the melt pool of newly deposited layer has a temperature much higher than the solidification temperature. However, at the overlapped layer, the melting temperature remains close to the solidification temperature. Owning to such a temperature gradient near the interface, the portion of non-mixing deposition flowed to melt pool, and was quickly concreted prior to mixing with fresh melt pool, which finally result in the formation of mixing zones or remelting zone. Fig. 4c further shows EDS line scanning results across the remelting zone of bimetallic structure. As can be seen, there exists a sharp compositional gradient for the Ni, Fe, Cr, Mo elements. Such elemental variation across the interface is believed to contribute to the heterogeneous distribution of microhardness in a narrow region, which will be discussed in the following section.

Fig. 5 further presents a quantitative analysis of the grains and elements segregation in interfacial regions. As shown in

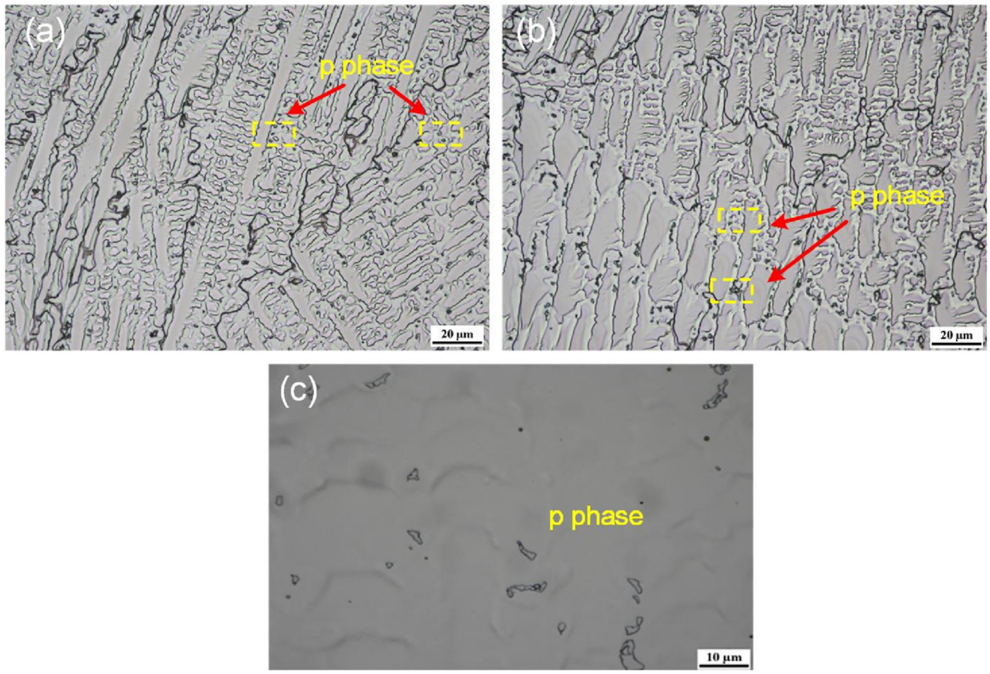

Fig. 3 – The p phase appearing in the interdendritic area of Hastelloy cladding: (a) as-fabricated state; (b) heat-treated state; (c) high-magnification optical micrograph.

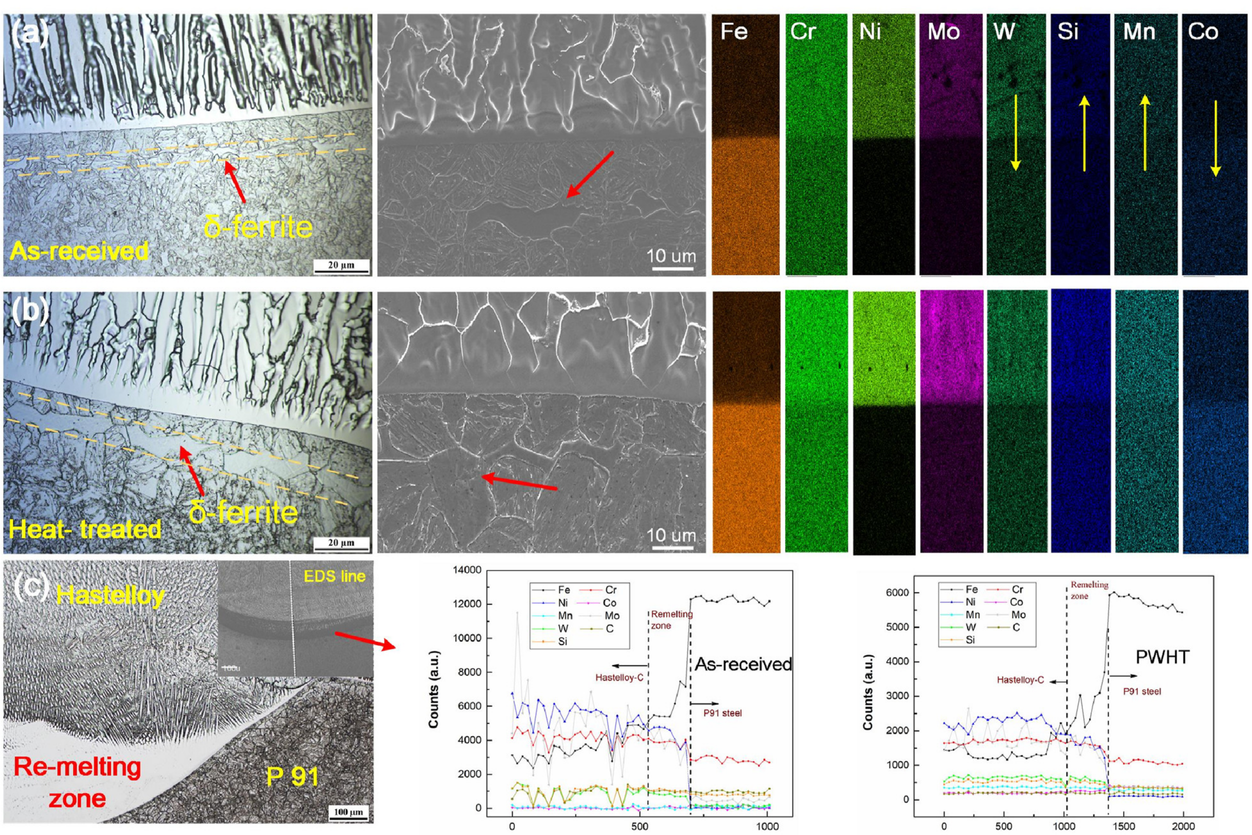

Fig. 4 – Interfacial features and elemental diffusion behaviour of: (a) as-cladded and (b) heat-treated specimens. (c) the re-melting zone shown in Fig. 2a.

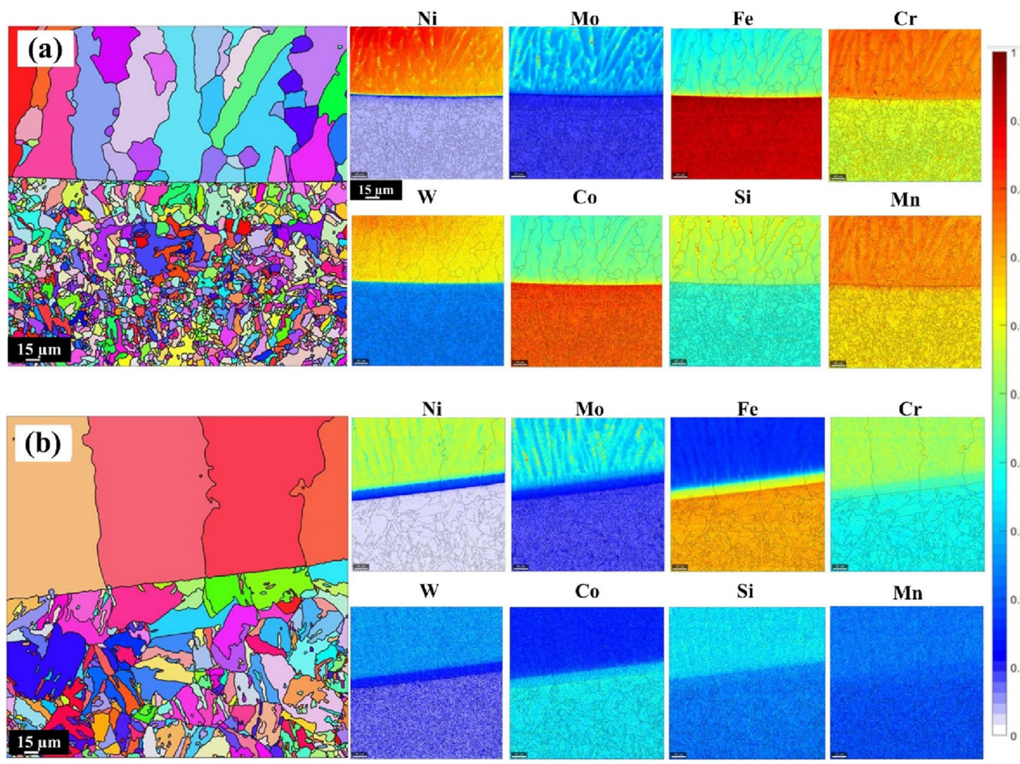

Fig. 5 – EBSD maps for interfacial elements distribution of: (a) as-cladded state and (b) heat-treated state.

Fig. 5a, it is displayed that Hastelloy C276 exhibits columnar grains of various sizes, and element Mo is segregated to the interdendritic areas. The P91 steel is characterized by tempered martensite. There is negligible change in its grain morphology, but the partial recrystallization that occurred during cladding thermal excursion led to grains growth. After heat treatment (Fig. 5b), the grains at both alloy sides are confirmed to be coarsened, and chemical segregations were homogenized in the microstructure. In the heat-treated state, the less pronounced segregation and coarse grains are beneficial for creep strength and corrosion resistance.

3.2. *Grain orientation and misorientation*

Fig. 6 presents EBSD orientation maps of two specimens at different conditions. In Fig. 6a and b, the <1 0 0> direction, as shown in arrows in the heat flow direction, determines the competitive grain growth [21]. It is well known that if the angle between heat flow and preferred crystallographic orientation is small, the favourably oriented grains grow faster, while other less-favourably oriented grains fall behind and will be suppressed. In the as-cladded condition, the coating grains (Hastelloy side) have great variation in their crystallographic orientation. However, there are occasional clusters of grains with the orientations <1 1 1> in the deposition direction (Fig. 6e), compared to building direction (Fig. 6c), which is associated with the fluctuations in thermal condition during cladding, instead of due to the cooling rate locally. For Hastelloy C276, the generation of <1 1 1> is relative to the symmetric twist boundaries during production, which strongly affects the extent of oxide film formation in the air environment [22]. This demonstrated the cladded surface would be slightly prone to oxidize due to the added grains aligned with <1 1 1> along the deposition direction. In the case of heat-treated state, there is a greater tendency for coating grains

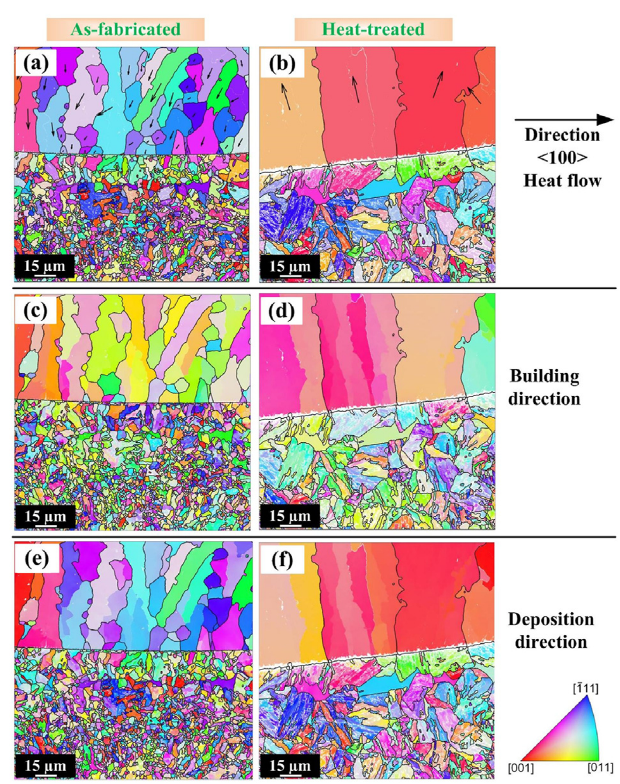

Fig. 6 – Inverse pole figure (IPF) maps of two specimens along the building direction and deposition direction.

to be columnar and to assume the preferred solidification growth direction of <0 0 1> aligned with both deposition direction (Fig. 6f) and building direction (Fig. 6d). Typically, the orientation <0 0 1> is the fast-growing dendritic orientation in Ni-based alloy and its growth is consistent with the anisotropy of solid–liquid interfacial energy [23]. Under stable thermal conditions, modified heat treatment could be desirable to promote the formation and coarsening of γ-Ni phases, while recrystallising as-cladded grains into the sequenced structure with <0 0 1> along the deposition direction. After heat treatment, the microstructure of substrate steel kept equiaxed grains, but also highly coarsened. It is well accepted that the microstructure has been significantly modified via post heat treatment.

Fig. 7 displays misorientation-angle distribution of selected locations under two studied conditions. Low-angle grain boundaries (LAGB) (2° < LAGB $<15^\circ$) and high-angle grain boundaries (HAGB) (HAGB $>15^\circ$) are depicted as black and red lines, respectively. Grain boundaries of both specimens are mostly composed of HAGBs and LAGBs. The HAGBs ratio is in a range of 87.7%–97.6% for as-cladded and heat-treated state. It is well known that the presence of a large amount of HAGBs in the microstructure is often beneficial for suppressing crack propagation or turning cracks to another direction, which could significantly improve mechanical strength or toughness response to the material, thereby extending the useable life of structure under a combination of load and high temperature conditions [24]. Since grain growth is present in heat-treated specimens, LAGBs have an obvious reduction. This demonstrates an improvement in ductility and resistance to cracking.

Fig. 8 exhibits the detailed misorientation of two samples at as-cladded and HT conditions. Figs. 8a and b shows Kernel Average Misorientation (KAM) images that could express local strain accumulation or dislocation slip in grains. From KAM map, the colour changes from blue to green and then to red, indicating that local KAM values increase successively. Higher KAM values could be found in the as-cladded state compared to heat-treated state. Figs. 8c and d further illustrates the local misorientation of two specimens, and the KAM values of most local misorientation are over 15, which indicates more plastic deformation or high defect density occurred. After heat treatment, there is a significant change in the residual plastic strain (Fig. 8b), especially in substrate steel. Due to grains deformation, KAM values seem to be homogeneously distributed at both sides. For coating layers (Hastelloy C276), high KAM values occurred in inner grain boundaries, which demonstrates inner grains firstly deformed when heat process begain. Dislocation activities at γ-Ni matrix also result in pronounced strain localization at the grain boundaries, as red areas (point) shown in Fig. 8a and b, where produced a number of new intermetallics. While, for P91 steel substrate, high KAM values appeared in the vicinity of the interface where undergone a large thermal gradient. It is evident that strain localization appeared during deposition, while it could be refined by heat treatment used in this study.

3.3. *Hardness distribution*

Fig. 9 shows a hardness map collected across the cladding to substrate. The hardness values are significantly determined by the microstructural evolution across the dissimilar materials. The high microhardness value appears in the CGHAZ due to the presence of untampered lath martensite and complete dissolution of carbides. After heat treatment, the overlay shows a decrease in average microhardness value from 250 HV to 220 HV, which is mainly attributed to the recovery and recrystallisation induced coarse grains (see Fig. 5). The hardness values in overall HAZ have an obvious reduction and became more homogenous compared to those without heat treatment (Fig. 9b), associated with the uniform microstructure. A similar observation has also been reported in previous research for hardness variation along the P91 HAZ in welded and post heat treatment [25]. The average hardness of P91 steel in the as-cladded state was measured at ~220 HV, while a slight 5% reduction was in heat-treated state. This is

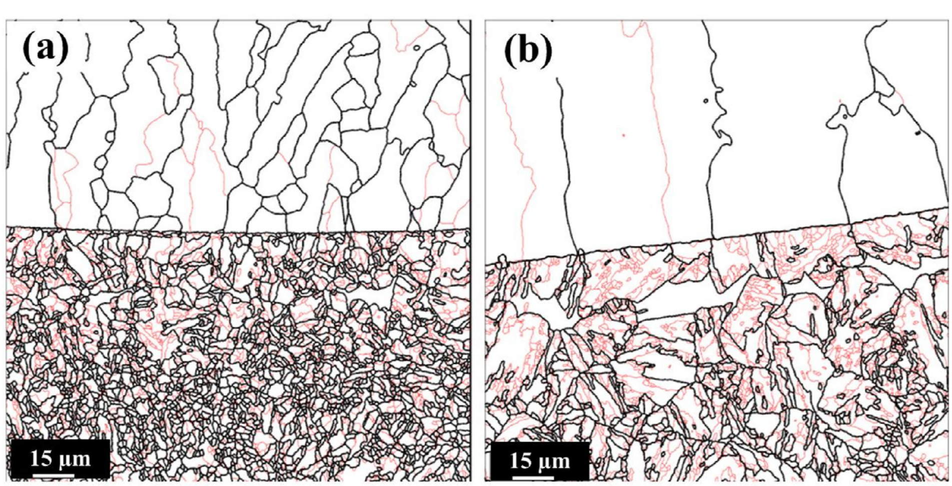

Fig. 7 – Grain boundaries maps of (a) as-cladded and (b) heat-treated conditions, LAGBs (2°–15°) in red, HAGBs (>15°) in black.

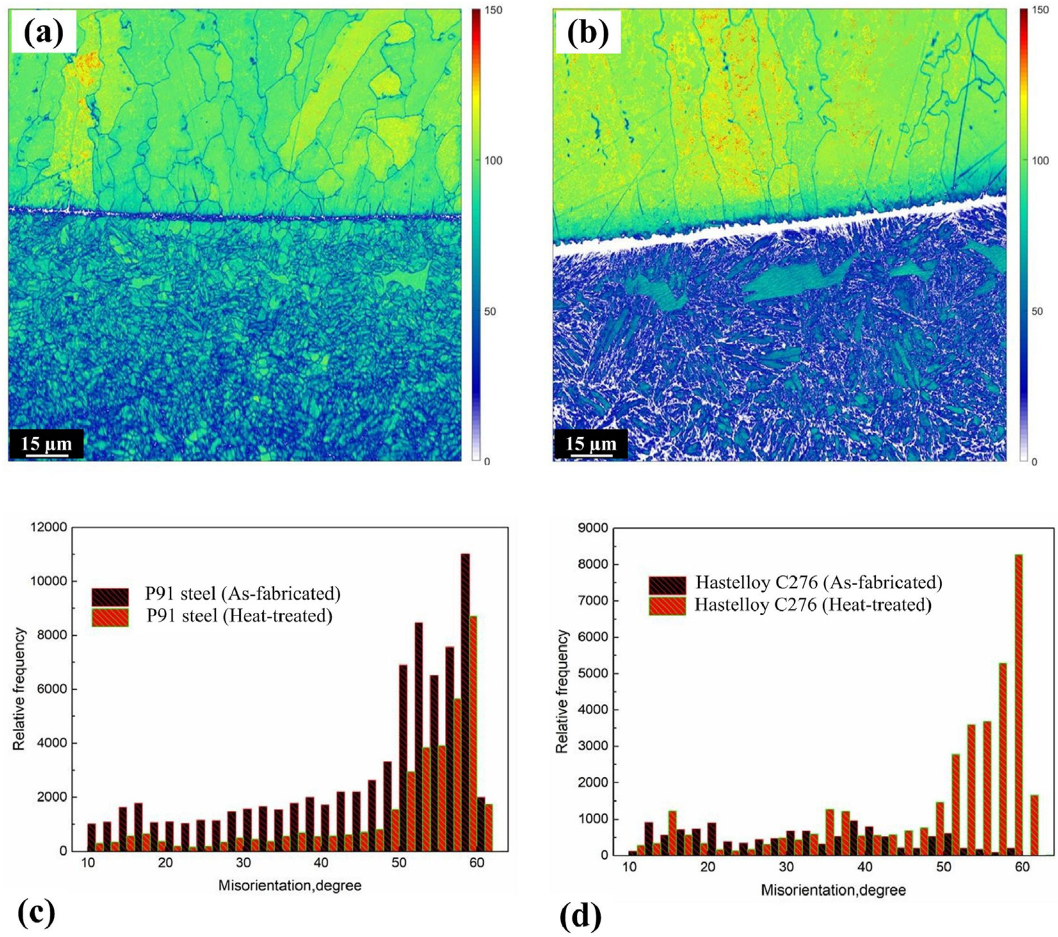

Fig. 8 – KAM image for (a) as-cladded state and (b) heat-treated state, and misorientation-angle distribution histograms for (c) P91 steel substrate and (d) Hastelloy C276 coating.

caused by further tempering of martensite (Fig. 2). Additionally, post-processing HT allowed microstructure homogenization and reprecipitation at CGHAZ, resulting in the reduction of the corresponding hardness. Here, it is mentioned that under the heat-treated condition used in this study, P91 steel has improved energy absorbing capacity, which could bring enhanced toughness to the material [9].

From the discussion above, it is well accepted that what this study prefers to display is the development of a new cladding structure for application in severe environments. It is believed that the analysis is beneficial to the study of Nickel-steel bimetallic components. The experiments under high temperatures and corrosion environments will be continued in the near future.

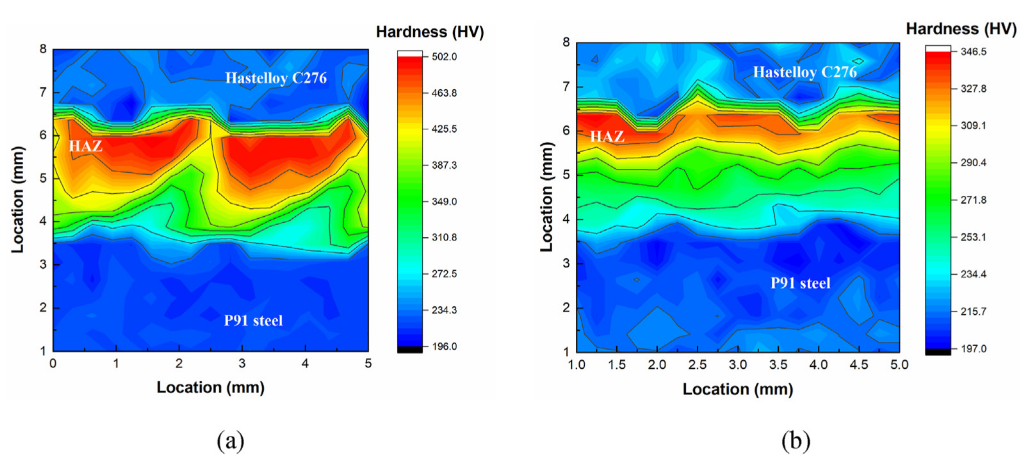

Fig. 9 – Hardness mapping of studied specimens: (a) as-cladded state; (b) heat-treated state.

4. Conclusion

A new dissimilar metal structure, where Hastelloy C 276 was claded on low-alloyed creep resistance steel P91 using wire arc additive manufacturing, has been successfully achieved in this study. A systematic microstructural characterization of specimen at as-cladded and heat-treated conditions was performed. The findings include:

(1) The proposed steel-nickel-based alloy bimetallic structure exhibits a sound bonding with microstructure hierarchies where columnar dendrites and *p* phase formed in cladding layer, and equiaxed martensite and carbides precipitation generated in steel substrate. The HAZ at interfacial bonding regions performs different grain sizes, possibly due to the alternatively thermal cycles and solute elements diffusion between dissimilar materials.
(2) The post heat treatment brings a significant change to microstructure at both Hastelloy C276 and p91 steel, including promoted grain growth, modified grain orientation, and enhanced HAGBs, which are critical to the overall property improvement. In particular, HAGBs in cladding may provide conditions against cracks generation and propagation.
(3) The various expressions of the hardness in different locations with and without post heat treatment can be explained by the combined effects of the grain size, crystallographic texture, grain boundaries as well as carbide distribution.

In sum, the study of material characterization of cladding Hastelloy C276 on P91steel enables a better understanding of steel-nickel based alloy bimetallic components for structural application.

Declaration of Competing Interest

The authors declare that they have no known competing financial interests or personal relationships that could have appeared to influence the work reported in this paper.

Acknowledgements

The authors wish to express appreciation for the financial support from Natural Science Foundation of Ningxia (No.2021AAC02001) and Ningxia key research and development plan (No. 2020BEB04021).

REFERENCES

[1] Grimes Rw KR, Edwards L. Greater tolerance for nuclear materials. Nat Mater 2008;7(9):683–5.
[2] Raabe D, Tasan CC, Olivetti EA. Strategies for improving the sustainability of structural metals. Nature 2019;575(7781):64–74.
[3] Wu B, Qiu Z, Pan Z, Carpenter K, Wang T, Ding D, et al. Enhanced interface strength in steel-nickel bimetallic component fabricated using wire arc additive manufacturing with interweaving deposition strategy. J Mater Sci Technol 2020;52:226–34.
[4] Zhang C, Zhang L, Shen W, Xu Q, Cui Y. The processing map and microstructure evolution of Ni-Cr-Mo-based C276 superalloy during hot compression. J Alloys Compd 2017;728:1269–78.
[5] Zhang X-y, Zhong J, Guo S-l, Zhao J. Control of deformation and annealing process to produce incoherent Σ3 boundaries in Hastelloy C-276 alloy. Nuclear Mater Energy 2021;27:100944.
[6] Zhang Q, Tang R, Yin K, Luo X, Zhang L. Corrosion behavior of Hastelloy C-276 in supercritical water. Corrosion Sci 2009;51(9):2092–7.
[7] Weber JH, Banerjee MK. Nickel and nickel alloys: an Overview☆, reference module in materials science and materials engineering. Elsevier; 2019.
[8] Pandey C, Mahapatra MM, Kumar P, Saini N. Comparative study of autogenous tungsten inert gas welding and tungsten arc welding with filler wire for dissimilar P91 and P92 steel weld joint. Mater Sci Eng, A 2018;712:720–37.
[9] Pandey C, Giri A, Mahapatra MM. Evolution of phases in P91 steel in various heat treatment conditions and their effect on microstructure stability and mechanical properties. Mater Sci Eng, A 2016;664:58–74.
[10] Grybėnas A, Makarevičius V, Baltušnikas A, Lukošiūtė I, Kriūkienė R. Correlation between structural changes of M23C6 carbide and mechanical behaviour of P91 steel after thermal aging. Mater Sci Eng, A 2017;696:453–60.
[11] Sridar S, Klecka MA, Xiong W. Interfacial characteristics of P91 steel - Inconel 740H bimetallic structure fabricated using wire-arc additive manufacturing. J Mater Process Technol 2022;300:117396.
[12] Hielscher R, Schaeben H. A novel pole figure inversion method: specification of the MTEX algorithm. J Appl Crystallogr 2008;41(6):1024–37.
[13] Qiu Z, Wu B, Zhu H, Wang Z, Hellier A, Ma Y, et al. Microstructure and mechanical properties of wire arc additively manufactured Hastelloy C276 alloy. Mater Des 2020;195:109007.
[14] Kumar S, Sirohi S, Vidyarthy RS, Gupta A, Pandey C. Role of the Ni-based filler composition on microstructure and mechanical behavior of the dissimilar welded joint of P22 and P91 steel. Int J Pres Ves Pip 2021;193:104473.
[15] Peng NG, Ahmad B, Muhamad MR, Ahadlin M. Phase transformation of P91 steels upon cooling after short term overheating above Ac1 and Ac3 temperature, advanced materials research. Trans Tech Publ; 2013. p. 1756–65.
[16] Messler Jr RW. Principles of welding: processes, physics, chemistry, and metallurgy. John Wiley & Sons; 2008.
[17] Mayr P, Cerjak H. The impact of welding on the creep properties of advanced 9–12% Cr steels. Trans Indian Inst Met 2010;63(2):131–6.
[18] Rajesh Kannan A, Mohan Kumar S, Pravin Kumar N, Siva Shanmugam N, Vishnu AS, Palguna Y. Process-microstructural features for tailoring fatigue strength of wire arc additive manufactured functionally graded material of SS904L and Hastelloy C-276. Mater Lett 2020;274:127968.
[19] Cheng X, Du Z, Chu S, Wu J, Dong J, Wang H, et al. The effect of subsequent heating treatment on the microstructure and mechanical properties of additive manufactured Hastelloy X alloy. Mater Char 2022;186:111799.
[20] Renuka Balakrishna A, James RD. A solution to the permalloy problem—a micromagnetic analysis with magnetostriction. Appl Phys Lett 2021;118(21):212404.

[21] Zhang X, Xu H, Li Z, Dong A, Du D, Lei L, et al. Effect of the scanning strategy on microstructure and mechanical anisotropy of Hastelloy X superalloy produced by Laser Powder Bed Fusion. Mater Char 2021;173:110951.
[22] Aliyu A, Sai Jyotheender K, Srivastava C. Texture and grain boundary engineering in nickel coating with tungsten addition and its effect on the coating corrosion behavior. Surf Coating Technol 2021;412:127079.
[23] D'Souza N, Ardakani MG, Wagner A, Shollock BA, McLean M. Morphological aspects of competitive grain growth during directional solidification of a nickel-base superalloy, CMSX4. J Mater Sci 2002;37(3):481–7.
[24] Kim S, Lee S, Lee BS. Effects of grain size on fracture toughness in transition temperature region of Mn–Mo–Ni low-alloy steels. Mater Sci Eng, A 2003;359(1–2):198–209.
[25] Pandey C, Mahapatra MM, Kumar P, Giri A. Microstructure characterization and charpy toughness of P91 weldment for as-welded, post-weld heat treatment and normalizing & tempering heat treatment. Met Mater Int 2017;23(5):900–14.